BMC Musculoskeletal Disorders

RESEARCH

Open Access

The link between osteoporosis and frozen shoulder: exploring the therapeutic effect of TAK715 on reversing fibrosis and protecting against osteoporosis via the p38 MAPK signaling pathway

Xinhao Li[1†], Yan Yan[1,2†], Zhuo Wang[1†], Jingyi Hou[1], Yuhan Meng[1], Dedong Cui[1], Yi Long[1*], Ming Li[1*] and Rui Yang[1*]

Abstract

Background The global incidence of frozen shoulder (FS) (2%~5%) and osteoporosis (OP) is high (9.1%-12.1%). Clinically, postmenopausal women are particularly at risk for both diseases. The main objective of this current research is to investigate the pathogenesis mechanism of FS and explore the connection between FS and OP.

Methods We obtained FS and OP datasets from GEO and identified crosstalk genes. Following KEGG and GO enrich analysis, the p38 MAPK signaling pathway was focused and the specific p38α inhibitor TAK715 was screened out. We conducted flow cytometry, western blot, and PCR analyses to assess the treatment effect of TAK715 on FS synovium fibroblasts at different concentrations. Additionally, we employed SD rats to validate the treatment effects of TAK715 in vivo.

Results TAK715 was useful in reversing fibrosis at the concentration of 1 μM, 5 μM and 10 μM. The unbalanced apoptosis process in frozen shoulder cell and the activation of osteoclast were inhibited at the concentration of 5 μM by TAK715. Then we successfully established a FS and OP rat model, with the FS with OP rat displaying less range of motion (ROM) and thicker shoulder capsule. In FS rat that was treated with TAK715, the frozen shoulder side was corrected in ROM and bone loss.

Conclusions The frozen shoulder with osteoporosis may exhibit more severe symptoms, and TAK715 is effective in protecting fibrosis and osteoporosis both in vitro and vivo. The therapy to correct FS and OP simultaneously by TAK715 provides novel approach in FS treatment and study.

Keywords Osteoporosis (OP), Frozen Shoulder (FS), P38 MAPK, TAK715

†Xinhao Li, Yan Yan and Zhuo Wang are co-first authors.

*Correspondence:
Yi Long
longy68@mail.sysu.edu.cn
Ming Li
liming76@mail.sysu.edu.cn
Rui Yang
yangr@mail.sysu.edu.cn
Full list of author information is available at the end of the article

Introduction

Frozen shoulder, or idiopathic adhesive capsulitis, is a prevalent condition affecting 2%–5% of the general population [1–3]. Individuals with this ailment endure increasing shoulder pain and a reduction in both active and passive range of motion (ROM) [4–6]. Several risk factors have been linked to the development of frozen shoulder, including diabetes mellitus, thyroid disorders, stroke, hyperlipidemia, and advancing age. The condition typically progresses through three distinct phases: the inflammatory and freezing stage, the frozen stage, and the thawing stage [4]. The average duration of symptoms before diagnosis is between 1 to 2.5 years [7–9]. While many patients may experience a full recovery, approximately 40% continue to suffer from significant pain and limited ROM [7, 8].

Current researches primarily focused on understanding the interplay between inflammation and the pathological fibrotic process [10–12]. However, the intrinsic characteristics of the synovial fibroblasts in frozen shoulder are less frequently discussed. The transition from the frozen to the thawing stage remains poorly understood, and there is no universally accepted mechanism [4]. Notably, studies have shown that the affected shoulder in frozen shoulder patients is more prone to osteoporosis compared to the healthy side [13, 14], yet this aspect is often overlooked. It's important to highlight that patients with osteoporosis often overlap in age with those with frozen shoulder, and there is evidence suggesting that frozen shoulder patients may be at risk for shoulder osteoporosis based on previous researches [15, 16].

Current studies have established that shifts in the shoulder joint environment towards a pro-inflammatory and pro-fibrotic state are pivotal [4]. Both intrinsic factors, such as changes in metabolic status [17, 18], and extrinsic factors, like trauma or surgery [19, 20], contribute to these environmental changes. For instance, patients with diabetes mellitus (DM) have a notably higher incidence of frozen shoulder, and matrix metalloproteinase (MMP) activity is suppressed in these patients [21, 22]. Extrinsic factors like trauma or surgery can trigger the release of cytokines such as IL-1β, IL-6, HMGB1, TNF-α, and TGF-β [12, 23, 24], which activate synovial fibroblasts (SFs) and lead to increased production of the extracellular matrix, including collagen I (Col I), collagen III (Col III), and fibronectin, thereby promoting fibrosis [24]. In this process, macrophages are drawn to the synovium by inflammatory signals and produce additional cytokines [25, 26]. Moreover, the persistent infiltration of macrophages and inflammatory cytokines can also stimulate osteoclast activation, potentially leading to local osteoporosis in the frozen shoulder [27–29].

The p38 MAPKs are activated by upstream MKK3 and MKK6 kinases and stimulate downstream targets such as p53, activating transcription factor 2 (ATF2), and myocyte-specific enhancer factor 2 (MEF2) [30, 31]. The p38 MAPK signaling pathway is implicated in various fibrotic diseases, including pulmonary, renal, bladder, and cardiac fibrosis. Inflammatory cytokines also activate p38, triggering subsequent responses [32, 33]. Active p38 has a pro-apoptotic role [34], and cell apoptosis is associated with fibrosis, as seen in liver fibrosis. Furthermore, osteoclast maturation is dependent on active p38 function [35, 36]. Given the cellular changes observed in the pathogenesis of frozen shoulder, we hypothesize that the p38 MAPK signaling pathway plays a critical role in this process. TAK715, an oral and potent p38 MAPK inhibitor with IC50s of 7.1 nM for p38α [37, 38], has been shown to ameliorate arthritis in rats [39] and may be an effective treatment to reverse fibrosis and protect against osteoporosis in frozen shoulder patients.

In this study, we initially analyzed clinical data to identify commonalities between frozen shoulder (FS) and osteoporosis (OP). We then explored the detailed mechanisms of FS and the link to osteoporosis by downloading FS and OP datasets from the GEO functional genomics database. Bioinformatic analysis revealed the MAPK signaling pathway as a key player in this interaction. Our experimental results corroborated these findings. Synovial fibroblast (SF) apoptosis was identified as a critical factor in fibrosis, and TAK715 was found to be effective in correcting apoptosis and fibrosis. In animal studies, we first confirmed that the affected side in FS patients was more osteoporotic than the healthy side. TAK715 was able to prevent FS and protect against osteoporosis in Sprague–Dawley rats. This study is the first to propose the simultaneous correction of fibrosis and osteoporosis in the treatment of FS patients, offering new insights into the pathogenesis of FS and its relationship with osteoporosis.

Materials and methods

Steps of experiments

First, bioinformatic analysis was performed to confirm different gene expression. KEGG and GO enrichment were then conducted based on the differentially expressed genes. After confirming previous studies and the drug's bioactivity, TAK715 was chosen as the therapeutic drug. Once the therapeutic effect of TAK715 had been confirmed on synovial fibroblasts (SFs) and osteoclasts maturation, the rats (*rattus norvegicus*, Sprague–Dawley) were selected as experimental animals due to their anatomical similarities and laboratory conditions. The schematic diagram of this study is shown in Fig. 1.

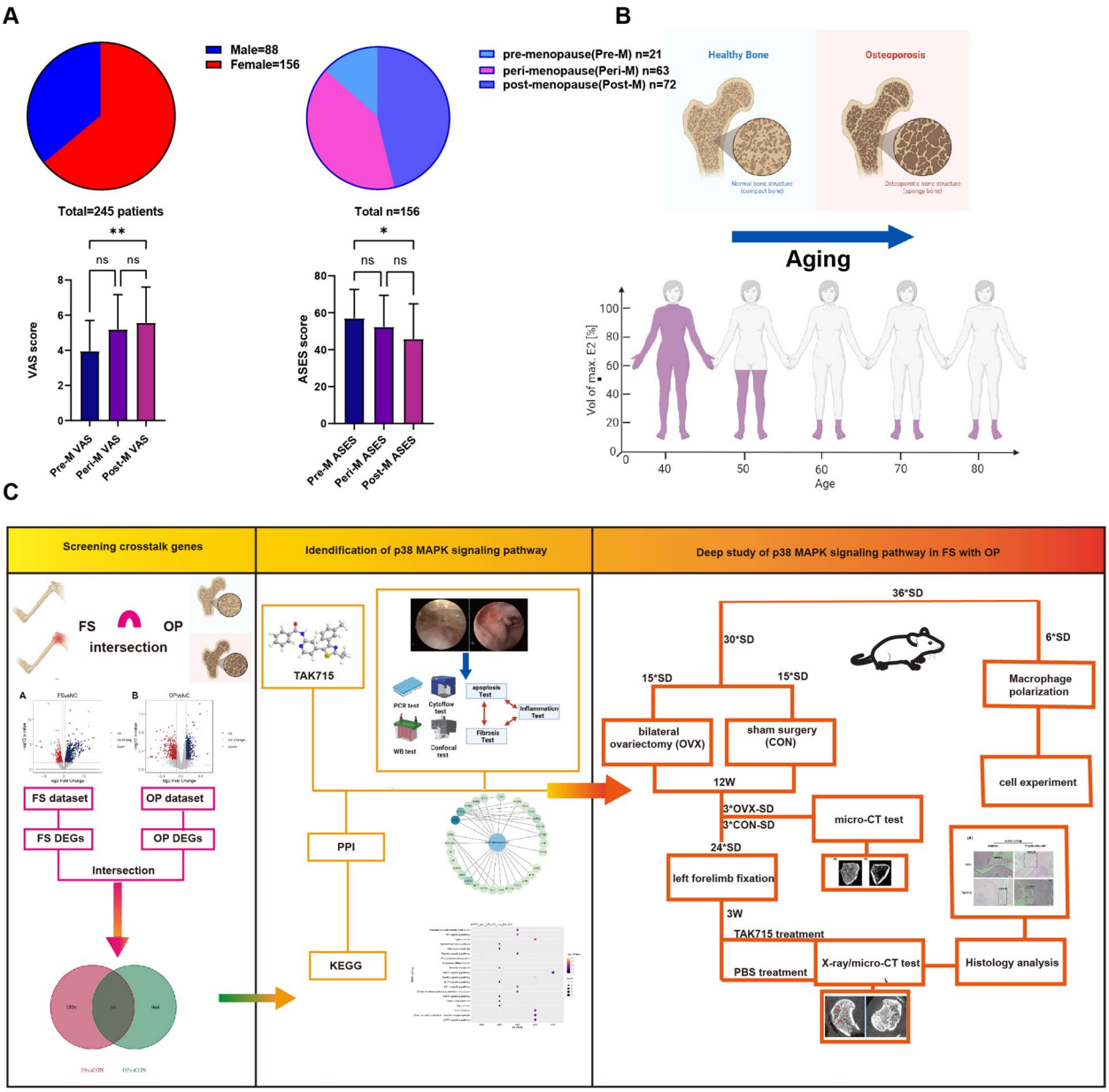

Fig. 1 The schematic diagrams of this study. **A**, **B** In the clinical setting, it was observed that the majority of frozen shoulder (FS) patients were women who had reached post-menopause (Post-M). Additionally, further investigation, including VAS (Visual Analog Scale) and ASES (American Shoulder and Elbow Surgeon) scores revealed that post-menopausal women tended to experience more severe symptoms. Considering the existing research, there is a strong association between post-menopausal women and osteoporosis (OP). The detailed patient baseline information was listed in Supplementary Table 1. Based on this observation, it was hypothesized that FS and OP might share common underlying mechanisms. **C** At first, the frozen shoulder (FS) dataset (GSE238053) that we uploaded before and osteoporosis (OP) dataset (GSE56815) were chosen to screen the crosstalk genes linking FS and OP. The p38 MAPK signaling pathway was screening out and the therapeutic effect was verified in vivo. In vitro, totally 36 SD rats were used in this study. First, 6 SD rats were sacrificed to harvest BMDMs. 15 SD rats received bilateral ovariectomy (OVX) and the other 15 SD rats received shame surgery (CON) simultaneously, Secondly, 3 OVX SD rats and 3 CON SD rats were sacrificed at 12 weeks after surgery to get the micro-CT scanning of femurs. The osteoporosis model was constructed successfully. Finally, we euthanized all residual SD rats to complete the ROM, micro-CT, X-ray test and the histological analysis

Data processing and bioinformatic analysis

GEO (https://www.ncbi.nlm.nih.gov/geo/) is a public genomics database that we obtained FS and OP dataset. The FS dataset (GSE238053) was performed in previous study [40]. The GSE56815 dataset was chosen as OP dataset to analysis, which was available and used in previous studies [41–43]. The detail information about above datasets was in Supplement Table 2. Considering the FS dataset, the original data was processed using the current method, and DEGs were selected using DESeq2 package with $|\log_2(\text{fold change})| > \log_2 1.5$ and p value < 0.05 by R package edgeR. In OP dataset, limma package was used and DEGs were selected with P-values < 0.05 and $|\log_2(\text{fold change})| > \log_2 1.1$ GO and KEGG enrichment analyses were then performed on the DEGs. Then the intersection DEGs were defined as crosstalk genes (Supplementary Table 3).

Synovial fibroblasts (SFs) isolation and culture from patients and controls

The FS patients were diagnosed based on physical examination, MRI imaging and medical history. The patients diagnosed with SLAP or dislocation were selected as the control group. The discard tissues were obtained through 3.5 mm grasping biopsy forceps during arthroscopy surgery.

The tissues isolated during arthroscopy were infiltrating in 0.9% saline solution immediately after being isolated in asepsis centrifuge tubes buried in ice. The tissues were then rinsed three times with Phosphate Buffered Saline (PBS) and cut into pieces. Next, the tissues were digested with 0.2 type 1 collagenase (MP) dissolved in high-glucose Dulbecco's modified Eagle's medium (high-glucose DMEM; Gibco, Thermofisher Scientific, Waltham, Massachusetts, USA). After being incubated at 37°C for 6 h, the SFs were collected through centrifugation at 1500 rpm/min for 5 min. The SFs were then resuspended in high-glucose DMEM containing 10% FBS and 1% Penicillin–Streptomycin Solution (complete DMEM) and transferred to a T25 culture flask for 7 days. The complete DMEM was changed every 3 days. The SFs were passaged when they reached 80–90% confluence, and the SFs from passages 4–6 were used for the following experiments.

Cell viability

The SFs were seeded in 96-well plate with 5×10^3 each well and incubated at 37°C with 5% CO2. The TAK715 was tested at the final concentration of 1 μM, 5 μM and 10 μM. When the cells were adhered, the primary medium was moved and the medium containing 10% CCK8(APeXBIO, Houston, USA) was added and incubated for 60 min. Finally, the 96-well plate was detected at the 450-nm absorbance using a microplate reader (Biotek Synergy H1M, Vermont, USA).

Synovial fibroblasts (SFs) identifications

The SFs were plated into a 6-well plate with 1×10^6 cells per well. Once the SFs had adhered, they were digested with trypsin and resuspended in PBS with 200 μl per well in a centrifuge tube. The experimental group was incubated with CD68(R&D Systems, Minnesota, USA) and Vimentin (R&D Systems, Minnesota, USA), while the negative control was incubated with only PBS for 20 min. Finally, the SFs were analyzed using flow cytometry with a Biosciences Influx cell sorter (BD, USA).

Quantitative real time polymerase chain reaction (qRT-PCR)

Total RNA from the SFs was isolated using the RNAQuick Columnar Purification Kit (EZBioscience, California, USA) and transcribed reversely into complementary DNAs using a reverse transcription master mix (EZBioscience, California, USA) according to the manufacturer's instructions. Quantitative real-time PCR was performed using SYBG Green Premix ((EZBioscience, California, USA). The data were normalized based on GADPH expression and the $2^{-\Delta\Delta Ct}$ method was used to analyze the relative expression of targeted genes. The forward and reverse primers for each interested gene are listed in Supplementary Table 5.

Western blot analysis

SFs were lysed using RIPA with proteinase inhibitor (1%) and phosphotransferase inhibitor (1%) (Cwbio, Jiangsu, China) and the protein concentrations were quantified with a protein assay kit (Cwbio, Jiangsu, China). Finally, samples were electrophoresed on 10% or 12% gels and then transferred to PVDF membranes (Millipore, MIT, USA).

The PVDF membranes were blocked with 5% BSA and incubated with primary antibodies overnight at 4°C. The following antibodies were used: Abcam (MA, USA): anti-Collagen I (1:1000), anti-Collagen III (1:1000), anti-Fibronectin (1:1000), anti-GADPH (1:3000), anti-caspase3 (1:1000). Huabio(Hangzhou, China): anti-p-p38(1:1000), anti-p38(1:1000), anti-Bax (1:1000). The membranes were then incubated with specific secondary antibodies for 1 h after washing 3 times by TBST. Finally, the analysis was performed using an ECL imager to get and analyze the signals.

Flow Cytometric Analysis of FITC Annexin V staining

The FITC Annexin V (BD Pharmingen™ FITC Annexin V Apoptosis Detection Kit I) was used to quantitatively determine the undergoing apoptosis according to the

BD protocol. The digested cells were washed twice with could PBS and then resuspend cells in Binding Buffer at a concentration of 1*10^6 cells/ml. The FITC Annexin V and PI were added to incubate for 15 min at 25°C in the dark. Then the flow cytometry analysis was performed within 30 min.

Enzyme-linked immunosorbent assays (ELISAs)

The concentrations of glenohumeral joint fluid samples were detected using vitamin B12 as an internal standard. A volume of 0.9 ml vitamin B12 was mixed with 4.1 ml 0.9% saline immediately before injection in darkness. Then, the mixtures were injected into the glenohumeral joint with a push-and-pull technique. The absorbances of samples were detected at $\lambda = 490$ nm and the dilution factors were calculated by comparing the absorbances. Finally, the concentrations of IL-1β, IL-6 and TNF-α were detected in both joint fluid and SFs culture supernatant using quantikine ELISA kits for human IL-1β, IL-6 and TNF-α (R&D Systems, Minnesota, USA) according to the guideline protocol.

Transwell migration assay

Cell migration assay was performed in Costar^{TM} 24-well plates (Corning, NY, USA) using Transwell^{TM}(Corning, NY, USA) inserts with polycarbonate membranes of 8.0 μm. Initially, the SFs culture medium were changed to culture medium without FBS for 24 h. Then $1x10^5$ cells of SFs were transferred to the inserts with 300 μl culture medium without FBS and 700 μl culture medium with 20% medium was added to the bottom of the 24-well plates well with treatment. After 24 h of incubation, the culture medium was moved carefully and the inserts were filtrated with 4% paraformaldehyde for 15 min and washed by PBS for 3 times. Then the inserts were stained with violet crystal (Byotime, Shanghai, China) for 5 min and washed by PBS for 3 times. Finally, the polycarbonate membranes were removed from the inserts to object slides and the visualizations analysis of the migratory cells were performed under the optical microscope using Image J.

RNA sequencing and bioinformatic analysis

Total RNA was isolated and purified using TRIzol reagent (Invitrogen, Carlsbad, CA, USA) following the manufacturer's procedure. The cDNA library was constructed and the average insert size for the final cDNA library was 300 ± 50 bp. At last, we performed the 2 × 150 bp paired-end sequencing (PE150) on an Illumina Novaseq$^{™}$ 6000 (LC-Bio Technology CO., Ltd., Hangzhou, China) following the vendor's recommended protocol.Then the original data was processed using the current method, and DEGs were selected using DESeq2 package with |log2(fold change) |> 1 and p value < 0.05 by R package edgeR. GO, KEGG and GSEA enrichment analyses were then performed on the DEGs. The detailed information and method were listed in Supporting information.

Osteoclasts culture and Macrophage polarization

The bone marrow derived macrophages (BMDMs) were cultured according to previous studies and seeded in a six-well plate with 5 × 105 per well and stimulated with rat macrophage colony stimulating factor (M-CSF, MCE, NJ, USA) at 30 ng/ml. Half of the medium was replaced by fresh complete medium with M-CSF every 48 h.

For osteoclasts inducements, the RANKL (MCE, NJ, USA) was added additionally at the final concentration of 50 ng/ml. Half of the medium was replaced by fresh complete medium with M-CSF and RANKL every 48 h.

For macrophage polarization, the BMDMs were treated into 3 groups. The negative control (NC) group was treated with PBS. To polarize M1 group. Lipopolysaccharide (LPS) and IFN-γ were dissolved in culture medium at a final concentration of 100 ng/ml and 20 ng/ml. The TAK715 treating group was set TAK715 at 5 μM while M1 polarization. Finally, the flow cytometry analysis was used to measure the typical markers of different group. The F4/80-APC (BD Bioscience, CA, USA) and CD86-FITC (BD Bioscience, CA, USA) were chosen as the typical index. The results were analyzed by FlowJo software.

Animal experiments

All animal procedures were approved by the Institutional Animal Care and Use Committee, Sun Yat-sen University according to ARRIVE guidelines [44]. Briefly, Frozen shoulder (FS), TAK715 treatment and osteoporosis were considered in the current study. All animals were randomly distributed into each group and the sample size were decided according to current researches [40, 45]. 6 groups, including osteoporotic confirming group (OC, $N=3$), control confirming group (CC, $N=3$), TAK715 treating FS osteoporotic group (T-FSOVX, $N=6$), FS osteoporotic group (FSOVX, $N=6$), TAK715 treating FS control group (T-FSCON, $N=6$) and FS control group (FSCON, $N=6$) were designed. The TAK715 treating was set as 10 mg/kg/day according to the previous studies and the control group was treated with PBS intraperitoneally. The SD rats was anesthetized with pentobarbital at the dose of 40 mg/kg before both surgery and sacrificed. After animals have been anesthetized and rendered unconscious, the method of cervical dislocation is employed to euthanize them. The detailed information about animal experiments was in Supporting information.

For the osteoporotic group, 15 SD rats were performed bilateral ovariectomy (Ovariectomize, OVX), which was

described previously. the rat was fasted from food and water for 12 h before surgery. The 15 mm median incision at the level of inguinal region at the abdomen was performed and bilateral ovaries were removed. Similarly, 15 SD rats received sham surgeries as control. The OC and CC group were sacrificed to identify the osteoporotic model using micro-CT scanning based on previous research 12 weeks after surgery.

For frozen shoulder (FS) group model, 24 SD rats received the left forelimb fixation under anesthesia. Briefly, plasters were cut into 5 cm-wide strips and made incisions to expose the right forelimb maintaining the normal movement. A total of 8-layer plasters were used to fixed the left forelimb. The TAK715 and PBS treating were performed as soon as the FS model initiation for continuous 3 weeks.

X-Ray examination

To verify the FS model and the treatment effect of TAK715, X-Rays were performed using Simens system under general anesthesia. First, the SD rats were placed on the scanning table in a prone position to obtain the neutral position images. Then, two 10 g weights were tied to the left and right forelimb of the rat using 5–0 nylon to acquire the abduction position images. The digital images were processed using photoshop software to measure the angle between the lateral scapular and the humerus.

Measurement of Glenohumeral range of motion (ROM)

The entire shoulder joints, including the forelimb and scapula were dissected from the rats after they were euthanized. First, the scapula was fixed using a 26G injection needle by penetrating the inferior and superior angle and a 26G injection needle was used to mark the humerus corresponding point. Similarly, the Glenohumeral ROM in neutral position was first measured and then the 10 g weight was tied to the forelimb to measure the Glenohumeral ROM in abduction position. The whole measuring procedure was performed within 10 min to maintain the biological activity of specimen. This method was based on previous literatures [45].

Micro-CT examination

Both 3 OVX and CON samples in 6 samples in each group harvested at each time point were scanned by micro-CT (Inveon, German) after fixation in 4% polyoxymethylene for 48 h. Images were acquired at an effective pixel size of 8.82 lm, a voltage of 80 kV, a current of 500 IA and an exposure time of 1500 ms in each of the 360 rotational steps to analyze the trabecular bone. The bone volume/total volume (BV/TV), bone surface area/bone volume (BSA/BV), trabecular thickness (Tb.Th, mm), trabecular number (Tb.N, 1/mm) and trabecular spacing (Tb.S, mm) were analyzed according to the guideline. Two-dimensional and three-dimensional trabecular bone structure image slices were reconstructed.

Statistical analysis

Data was expressed by mean ± standard deviation. The Student's t-test were performed to evaluate the differences between group. A statically significant difference was determined when one-tail P value < 0.05. The SPSS 23.0 software (Chicago, IL, United States) was used during statistical analysis.

Results

p38 MAPK signaling pathway linked FS and OP as key crosstalk genes

Differential gene expression (DEG) analysis was conducted using the limma and DEseq2 packages to identify DEGs in frozen shoulder (FS) and osteoporosis (OP). Volcano plots and heatmaps were utilized to visualize these DEGs (Fig. 2). Additionally, Gene Ontology (GO) enrichment analysis and Kyoto Encyclopedia of Genes and Genomes (KEGG) pathway analysis were performed on the FS and OP datasets separately.

In the KEGG pathway analysis for FS, the top 5 pathways identified were the PI3K-Akt signaling pathway, MAPK signaling pathway, cGMP-PKG signaling pathway, cell adhesion molecules (CAMS), and Rap1 signaling pathway (Fig. 3D), which is partially consistent with a previous study [12]. Notably, the gene ratio analysis confirmed the significance of the MAPK signaling pathway in the fibrotic process of synovial fibroblasts from FS patients. The GO biological process (BP) analysis also

(See figure on next page.)

Fig. 2 Gene expression change during the pathological process of FS and OP. **A**, **B** The volcano plot of different expression genes in frozen shoulder (FS) group compared with control group (NC) and osteoporosis (OP) compared with control group (NC). The volcano plot was constructed with fold-change values (log2 scale) and *p* values (-log10 scale). The vertical lines were corresponding with the $\log_2$ fold change of $\log_2$1.5 in A and $\log_2$1.1 in B. The horizontal line represents with a *p* value of 0.05 in both A and B. **C**, **D** The heatmap of the top 1000 DEGs in FS and OP dataset. **E** Top 20 GO BP terms of DEGs in FS dataset. The positive regulation of MAPK cascade was involved. **F** Top 20 GO BP terms of DEGs in OPdataset. **G** Top 20 KEGG pathways of DEGs in FS dataset. **H** Top 20 KEGG pathways of DEGs in OP dataset. **I** The Venn diagram of intersection of FS and OP DEGs. **J** Top 20 KEGG pathways of intersection DEGs. **K** Top 20 GO BP terms of intersection DEGs. **L** The PPI network analysis of intersection DEGs. The shade of color represented the MCODE betweeness score and the MAPK singaling pathway took over the core regulation in crosstalk genes

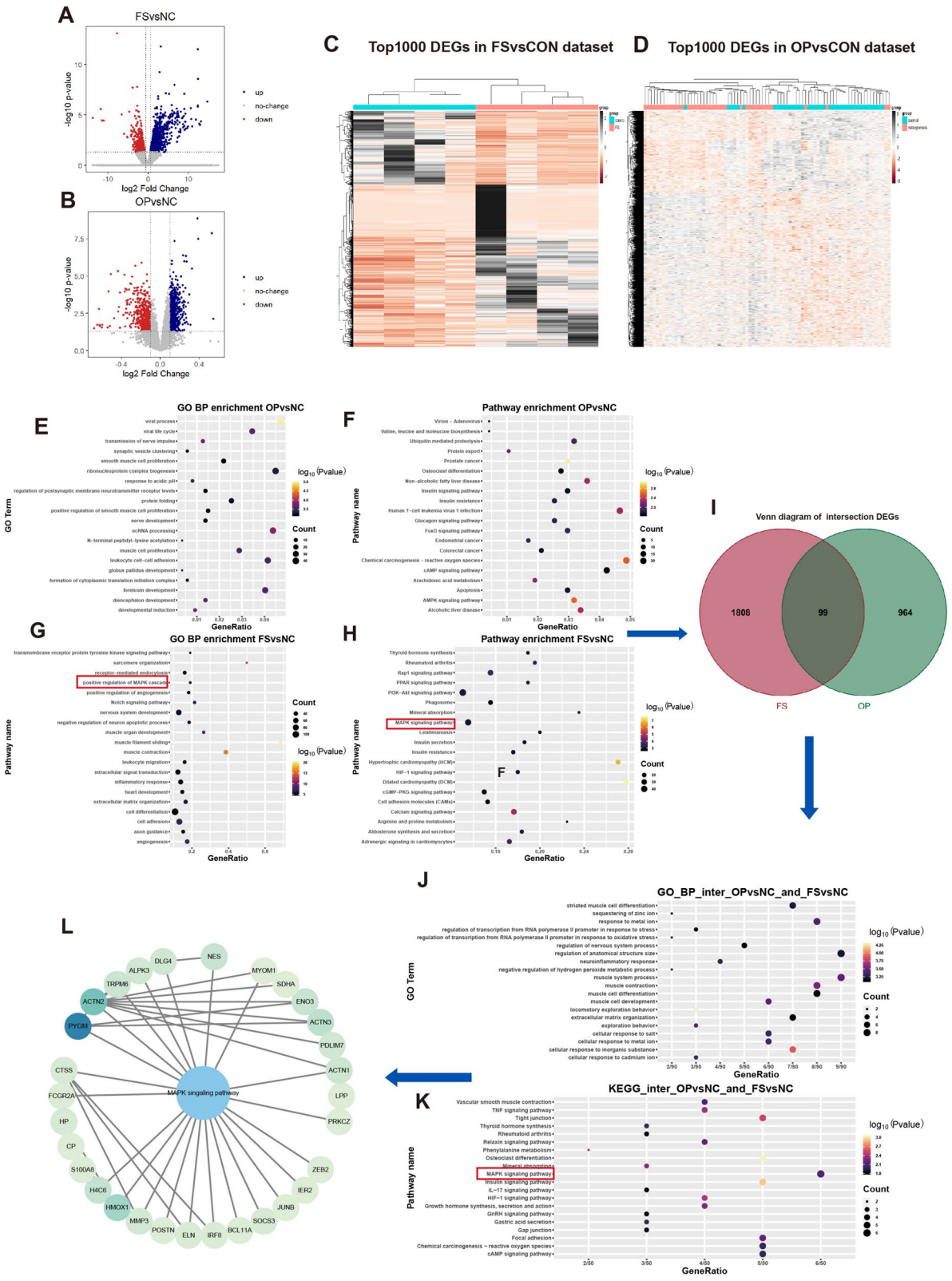

Fig. 2 (See legend on previous page.)

supported the role of positive regulation of the MAPK cascade, aligning with the KEGG analysis. In the OP KEGG analysis, the MAPK signaling pathway was among the top 50 pathways with a p-value of 0.0256 and a gene count of 25 (Supplementary Table 4).

To explore the link between FS and OP, we screened the intersection of DEGs from both conditions and identified crosstalk genes. The intersection KEGG pathway analysis revealed significant enrichment of the MAPK signaling pathway with the highest gene ratio (Fig. 2K). The protein–protein interaction (PPI) network analysis suggested that the MAPK cascade may play a central regulatory role among the crosstalk genes (Fig. 2L). For example, the MAPK cascade could regulate MMP3 expression [46] and activate POSTN [47]. Our bioinformatic analysis confirmed the vital role of the MAPK signaling pathway in the pathogenesis of both FS and OP, as well as its significant involvement in the crosstalk genes.

Identification of frozen shoulder (FS) tissue and synovial fibroblasts (SFs)

During arthroscopic surgery, the synovium in frozen shoulder (FS) patients exhibited hyperemia and inflammation, with a distinctly thickened joint capsule observable under arthroscopy (Fig. 3A). The pathological hallmark of FS is characterized by pathological fibrosis. To assess the tissue and molecular level pathological processes, synovial samples from FS patients and control patients (with SLAP lesions or dislocations) were collected arthroscopically. Collagen I and Collagen III, known markers of fibrosis, were selected to evaluate the degree of fibrosis in the synovium of FS patients. Immunohistochemical analyses revealed significantly higher expression of these proteins in the synovium of FS patients compared to control patients, indicating a higher degree of fibrosis in the FS synovium (Fig. 3B, C).

Having identified the tissue, primary synovial fibroblasts (SFs) isolated from FS and control patients were further characterized. The SFs utilized in this study were derived from the synovium and passaged to 4–6 generations. Phenotypic analysis of FS by flow cytometry demonstrated that SFs from both FS and control patients predominantly expressed vimentin and were negative for CD68, consistent with previous studies [12, 40, 48] (Fig. 3D).

p38 MAPK signaling pathway exhibits important effect in pathological fibrosis of FS patients

The MAPK signal pathway, which mainly consists of ERK, Jun, and p38 MAPK, has been shown to be significantly important in fibrotic diseases such as renal fibrosis and pulmonary fibrosis. Previous studies have confirmed that the active form of p38 MAPK is mainly the phosphorylation of p38 MAPK (p-p38), and that TAK715 is a specific effective p38α inhibitor that is orally active, indicating its potential clinical value. The IHC results showed that p-p38 was expressed at higher levels in FS synovium than in the control group at the tissue level (Fig. 3G, H). Moreover, western-blot analysis suggested that the phosphorylation level of p38 in FS fibroblasts was significantly higher than that in control fibroblasts (Fig. 3E, F).

Based on previous studies [34], the overactivation of p38 MAPK is positively linked to the imbalance of cell apoptosis, which could trigger pathologic diseases such as liver fibrosis. To explain the detailed mechanism of pathological fibrosis in FS, we compared the cell apoptosis process in FS and control groups. First, the caspase-3 and Bax were selected as primary indices to respond to the apoptosis level. The IHC and western-blot results showed that caspase-3 and Bax were all expressed at higher levels in FS than in control group (Fig. 3E-H). The tunnel staining and flowcytometry analysis also confirmed that the apoptosis process was more dynamic in FS than in the control group (F ig. 3I-K). The above results confirmed that cell apoptosis played a key role in the FS fibrosis process from the molecular to the tissue level.

(See figure on next page.)

Fig. 3 The FS tissue was successfully collected and digested into FS synovium fibroblasts. Besides phosphorylation level of p38 was higher and cell apoptosis was more active in the FS group. **A** The arthroscope view of Control (**a**,**b**) and FS(**c**,**d**) patient: the capsular was more thicken and the synovium was hyperemia and inflammation infiltrated. **B** Representative Collagen I and Collagen III immuno-stained tissue sections in control and FS tissue. Scale Bar: 50 μM. **C** The statistics analysis of (**B**): the mean optical density (mean OD) of Collagen I and Collagen III in the control and FS tissues ($n = 3$). **D** The representative flow cytometry results of synovial fibroblasts and the statistic results ($n = 3$). **E**, **F** The western blot analysis of Collagen I, Collagen III, p-p38, Caspase-3 and Bax. The statistic results ($n = 3$) confirmed that the above proteins were higher expressed in the FS group, which were corresponding with the IHC results. *$P < 0.05$; **$P < 0.01$; *** $P < 0.001$; **** $P < 0.0001$. **G** Representative p-p38, Caspase-3 and Bax immuno-stained tissue sections in control and FS tissue. Scale Bar: 50 μM. **H** The statistics analysis of (**A**): the mean optical density (mean OD) of p-p38, Caspase-3 and Bax in the control and FS tissues ($n = 3$). *$P < 0.05$; **$P < 0.01$; *** $P < 0.001$; **** $P < 0.0001$. **I**, **J**, **K** The cell apoptosis was more active in FS group based on the Tunel staining (**I**) and flow cytometry analysis (**G**). Scale Bar: 200 μM. *$P < 0.05$; **$P < 0.01$; *** $P < 0.001$; **** $P < 0.0001$

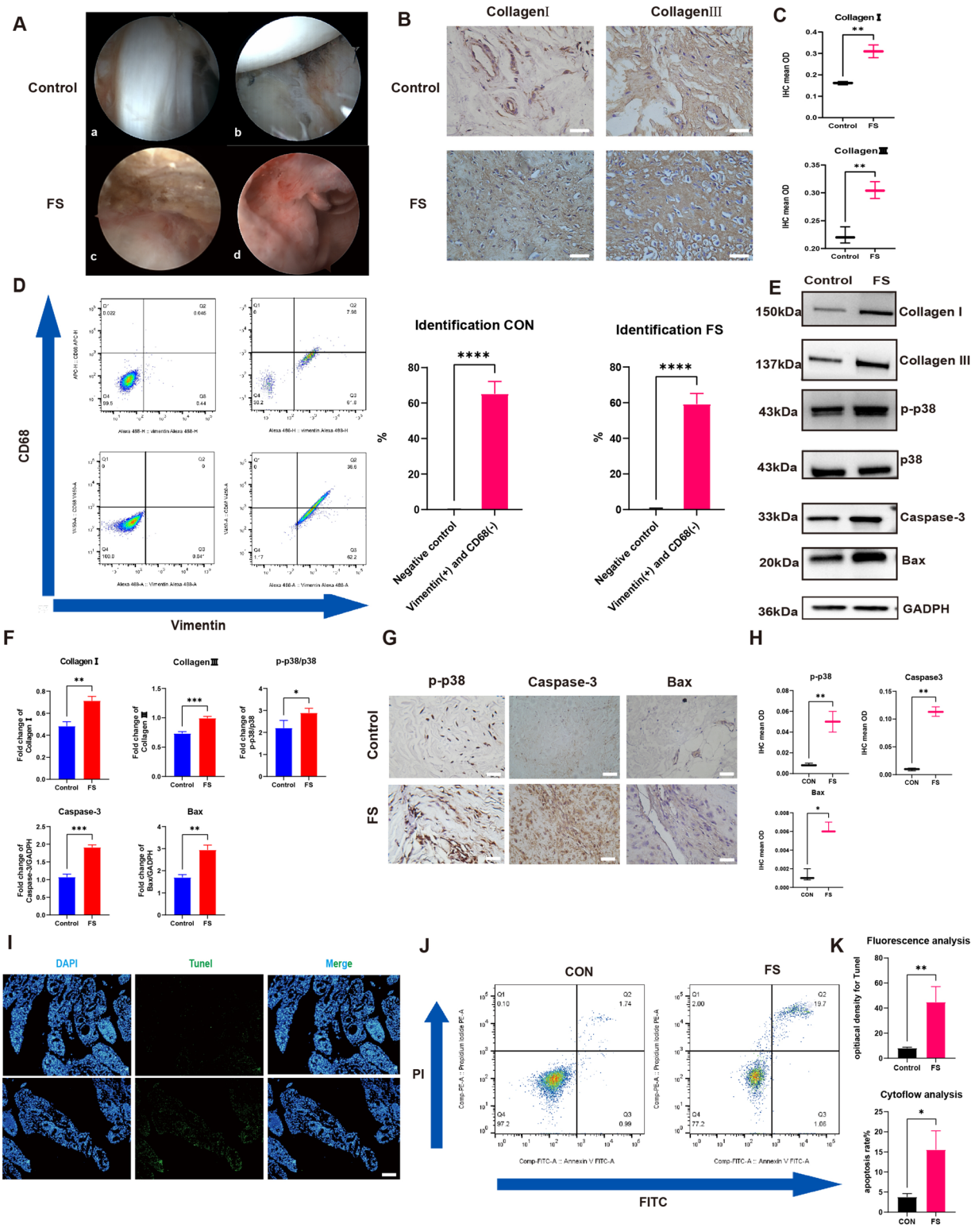

Fig. 3 (See legend on previous page.)

TAK715 is safe and effective in reversing the fibrosis process of FS fibroblasts through protecting imbalanced cell apoptosis

Since p38 MAPK signaling pathway was unusually active, the specific p38 inhibitor TAK715 was chosen as treatment. First, we used CCK-8 reagent to test the TAK715 on the viability of synovial fibroblasts (SFs). The results indicated that there was no significant change in the SFs viability after the addition of TAK715 at the final concentration of 1 μM,5 μM or 10 μM (Fig. 4A). We then interfered the synovial fibroblasts that were digested from FS patients with TAK715 at the final concentration of 1 μM,5 μM and10μM for 24 h. First, the qRT-PCR and western-blot analysis suggested that the TAK715 could significantly inhibit the phosphorylation of p38 in SFs with TAK715 at 1 μM,5 μM and 10 μM. Especially, the inhibition rate was higher at the concentration of 5 μM and 10 μM than 1 μM (Fig. 4B-D).

Furthermore, the expression levels of Fibronectin, Collagen I and Collagen III decreased significantly after the interference of TAK715 at the above conditions, as confirmed by both western-blot and qRT-PCR analysis. The TAK715 was more effective in reversing the fibrosis process at the concentration of 5 μM and 10 μM than 1 μM. Additionally, since the degree of fibrosis is positively linked to cell migration ability, we performed scratch tests and transwell migration assays. In transwell migration assay, the migrated SFs through the polycarbonate membrane with the interference of TAK715 at the above conditions were all significantly decreased compared with the FS group. Both the scratch test and transwell migration assay were consistent with the western-blot and qRT-PCR analysis (Fig. 4E).

To further explore the mechanism behind TAK715's ability to reverse the fibrosis process in FS synovium fibroblasts, we also checked the cell apoptosis indexes. The western-blot analysis indicated that the caspase-3 expression level was lower in the TAK715 group than in the FS group at the above conditions. However, the TAK715 showed no significant inhibition effect on Bax at the concentration of 1 μM (Fig. 4F and H). Based on the western-blot analysis, we chose a TAK715 concentration of 5 μM to perform the cell flowmetry analysis, and the results confirmed that TAK715 could significantly protect the imbalanced apoptosis in FS synovium fibroblasts (Fig. 4G and I).

These results confirmed that TAK715 was safe at concentrations of 1 μM, 5 μM, and 10 μM, and at these concentrations, TAK715 could effectively reverse the fibrosis process of FS fibroblasts. In particular, TAK715 was more effective at concentrations of 5 μM and 10 μM than at 1 μM. Furthermore, TAK715 could protect the imbalanced apoptosis in FS synovium fibroblasts at concentrations of 5 μM and 10 μM.

The TAK715 could prevent the macrophage polarization and interfere the SF fibrosis during TNF-α stimulation

During arthroscopic surgery, we observed inflammation infiltration in the synovial tissue of frozen shoulder (FS) patients, prompting us to investigate the pro-inflammatory role of M1 macrophages. Using CD86 as a characteristic marker for M1 macrophages, we discovered a higher prevalence of CD86-positive macrophages in FS synovial tissue compared to the control group (Supplementary Fig. 1B). Additionally, we quantified the levels of cytokines IL-1β, IL-6, IL-10, and TNF-α in the glenohumeral joint of patients using ELISA. The concentrations of these cytokines were significantly elevated in the joints of FS patients, with TNF-α exhibiting the most pronounced difference (Supplementary Fig. 1.C). Furthermore, we explored the impact of TAK715 on macrophage polarization and found that TAK715 could inhibit M1 macrophage polarization at a concentration of 5 μM under LPS and IFN-γ stimulation, as shown by flow cytometry results, thereby reinforcing its anti-inflammatory effect (Fig. 4J). These findings suggested that

(See figure on next page.)

Fig. 4 The TAK715 was safe and could reverse the fibrotic process of FS synovium fibroblasts and the inappropriate SFs apoptosis was inhibited during this process. Moreover, the TAK715 showed remarkable anti-inflammatory effects. **A** The flowchart of the fibrosis and inflammation experiments. **B** The CCK 8 analysis confirmed the TAK715 was safe for synovium fibroblasts at the concentration of 1 μM, 5 μM and 10 μM. **C**, **D** The western blot analysis of the TAK715 effect on reversing the fibrotic process of FS synovium fibroblasts. The statistic results ($n=3$) confirmed that the TAK715 could reverse the fibrotic process of FS synovium fibroblasts at the final concentration of 1 μM, 5 μM and 10 μM. *$P<0.05$; **$P<0.01$; *** $P<0.001$; **** $P<0.0001$. **E** The transwell analysis confirmed the TAK715 could decrease the migration ability of FS synovium fibroblasts, which was consistent with the western-blot analysis. Scale bar: 1000 μM. *$P<0.05$; **$P<0.01$; *** $P<0.001$; **** $P<0.0001$. **F**, **G**, **H**, **I** the TAK715 could inhibit the FS synovium fibroblasts apoptosis at the effective concentration of 5 μM and 10 μM in western-blot (F)(H) and flow cytometry analysis(G)(I). **J** the flow cytometry of the TAK715 effect on inhibit the M1 polarization. **K**, **L** The western blot analysis of the TNF-α stimulating the control synovium fibroblasts into the fibrotic process and the TAK715 could inhibit this stimulation on synovium fibroblasts. The statistic results ($n=3$) confirmed that the TNF-α could stimulate the control synovium fibroblasts into the fibrotic process at the final concentration of 100 ng/mL significantly and the TAK715 could inhibit this process at 5 μM effectively. **M**, **N** the confocal image showed that under the stimulation of TNF-α at 100 ng/mL the p65 enter the cell nuclear to perform the subsequent process and the TAK715 could interpose this process at 5 μM. Scale Bar: 50 μm. *$P<0.05$; **$P<0.01$; ***$P<0.001$; ****$P<0.0001$

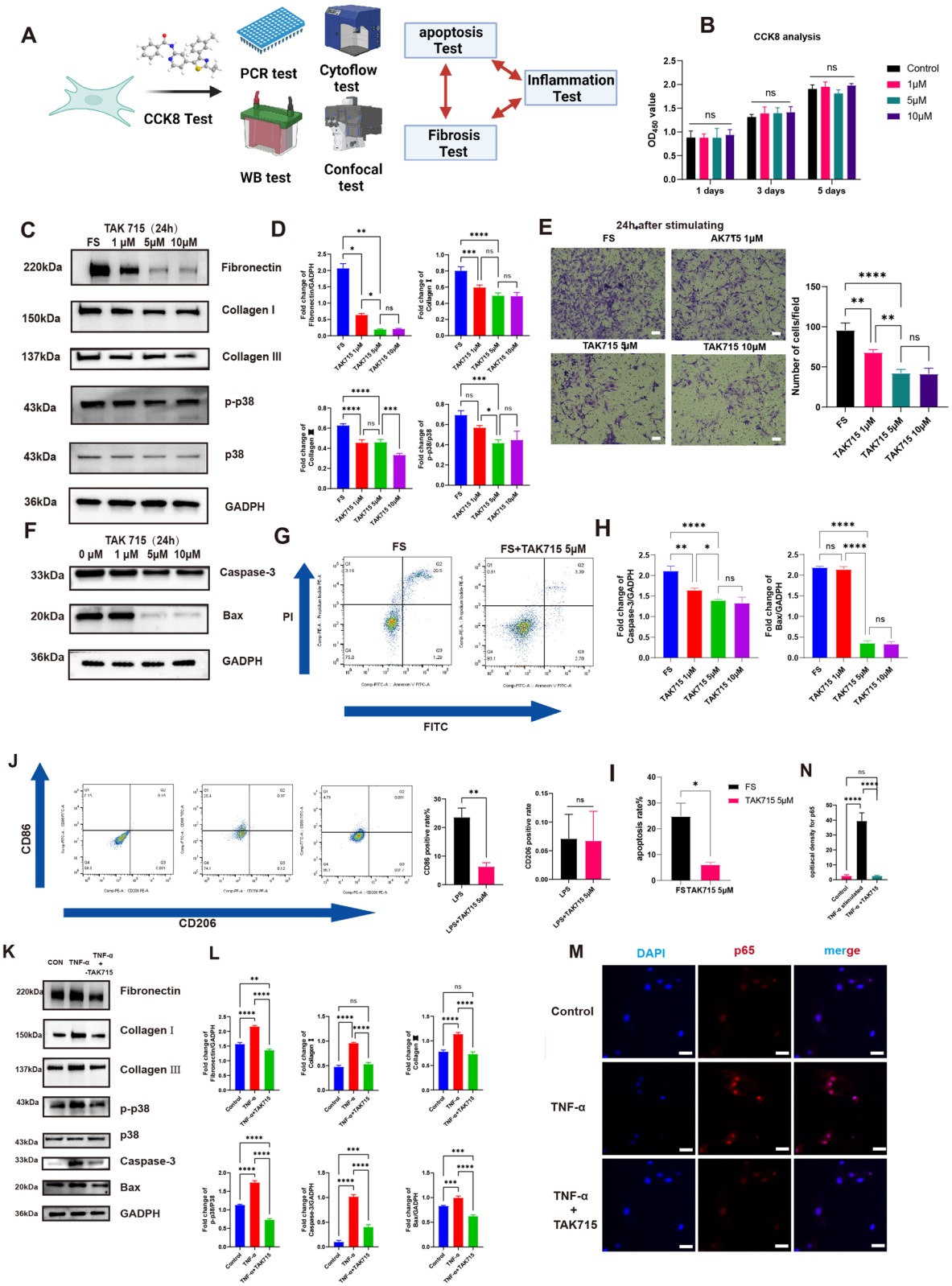

Fig. 4 (See legend on previous page.)

pro-inflammatory cytokines could initiate the fibrotic process in FS, and that TAK715 effectively counters inflammatory responses.

Building on these results and prior research, we selected TNF-α to stimulate synovial fibroblasts from control patients at a concentration of 100 ng/ml [49–51]. We then applied TAK715 at a concentration of 5 μM to verify its anti-inflammatory properties. qRT-PCR and western-blot analysis revealed significant upregulation of fibronectin, collagen I, and collagen III when these cells were stimulated by TNF-α (Supplementary Fig. 1.D, Fig. 4K-L). Moreover, apoptosis indices were also significantly elevated under this stimulation (Fig. 4K-F), indicating that pro-inflammatory cytokines might enhance SFs apoptosis, thereby initiating the fibrosis process.

To delve deeper into the mechanism behind TAK715's anti-inflammatory effect, we assessed its capacity to prevent p65 from translocating into the cell nucleus and initiating downstream effects under the LSM 5 Exciter confocal imaging system. The confocal imaging confirmed that TAK715 could indeed impede the subsequent functional role of p65 (Fig. 4M, N). These results provided valuable insights into the molecular mechanisms of TAK715's anti-inflammatory action and its potential therapeutic utility in mitigating the inflammatory processes associated with FS.

The bioinformatic analysis confirmed the reverse-fibrosis and anti-inflammation effect of TAK715 through specific signaling pathways

To investigate the gene expression under TAK715 stimulation in FS synovial fibroblasts and further clarify the therapeutic effect of TAK715 on FS synovial fibroblasts, we consequently performing the RNA-seq technology to examine the synovial fibroblast transcriptome from 6 individuals with FS (The FS group was set as negative control group, NC group) and 3 of these were stimulated with TAK715 at 5 μM (TAK5 group). We identified 2068 differentially expressed genes (DEGs) (1153 significantly up and 915 significantly down) with $|\log_2\text{fold change}| > \log_2 2$ and adjusted p-value < 0.05 between the NC and TAK5 group (Fig. 5A). The enrichment analysis, including GO, KEGG and GSEA analysis were performed to investigate the functional implications of TAK715 in FS synovial fibroblast. In GO analysis, the extracellular region (GO:0005576), extracellular space (GO:0005615) and cell junction (GO:0030054) in Cellular Component showed that the TAK715 could adjust the extracellular component, as the FS synovial fibroblasts synthesize and secret more extracellular matrix. In GO biological process, the apoptosis process (GO:0006915) in top20 enriched gene number and apoptosis pathway in KEGG (pathway ID: hsa04210) exhibited that the TAK715 could interfere the apoptosis process in FS synovial fibroblasts. Considering the inflammation effect on synovial fibroblasts, the TNF (pathway ID: hsa04668) and IL-17 (pathway ID: hsa04657) signaling pathways in KEGG analysis are significantly enriched, which indicated that the TAK715 interposed the inflammation response in FS synovial fibroblasts. The bioinformatic analysis in both extracellular and inflammation response is corresponding with previous part of this study (Figs. 5 and 6).

Subsequently, the GSEA analysis further discuss the relationship between certain pathways. The interested pathways were focused within the p value < 0.05, FDR (false discovery rate) < 0.25 and |NES| > 1. In KEGG enrichment analysis, considering the previous part in this study, we analysis the MAPK signaling pathway and apoptosis. The GSEA results verified that the TAK715 could lessen the MAPK cascade activity and remit the FS synovial fibroblasts apoptosis. Considering the inflammation and fibrosis aspect, the IL-17, TNF and TGF-βsignaling pathways GSEA results exhibited the anti-inflammation and anti-fibrosis effects of TAK715, corresponding with previous part in this study. Additionally, in GO term GSEA analysis, we emphasized on collagen-related terms. The collagen binding, collagen-containing extracellular matrix, collagen fiber organization, growth factor activity and collagen trimer term results showed the TAK715 effect on reversing fibrosis, which is also consistent with previous part.

(See figure on next page.)

Fig. 5 Gene expression after the treatment of TAK715. **A** The volcano plot of different expression genes after the TAK715 treatment at 5 μM in FS synovial fibroblasts. The untreated FS synovial fibroblast was set as control group (NC) and the FS synovial fibroblasts that were treated with 5 μM TAK715 (TAK5) was set as compared group. The volcano plot was constructed with fold-change values (log2 scale) and p values (-log10 scale). The vertical lines were corresponding with the $|\log_2$ fold change $|$of $\log_2 2$ and the horizontal line represents with a p value of 0.05. **B** The heatmap of the top 1000 DEGs in this gene set. **C** The GO Enrichment BarPlot of DEGs (ranked by enriched gene numbers). The terms that we focused were highlight. In top20 biological process, the apoptotic process (GO:0006915) was included. In top10 Cellular Component, the extracellular region (GO:0005576), extracellular space (GO:0005615) and cell junction (GO:0030054) were included. In Molecular Function, the protein binding (GO:0005515) was included. **D** The top20 KEGG pathways (ranked by *p*.value). The terms that we focused were highlight. The IL-17 signaling pathway (hsa04657), TNF signaling pathway (hsa04668) and apoptosis (hsa04210) were included. **E**, **F** The top 30 *P* Value of GSEA Enrichment analysis in KEGG and GO. The pathways or terms that we focused were highlighted. NES: normalized enrichment score

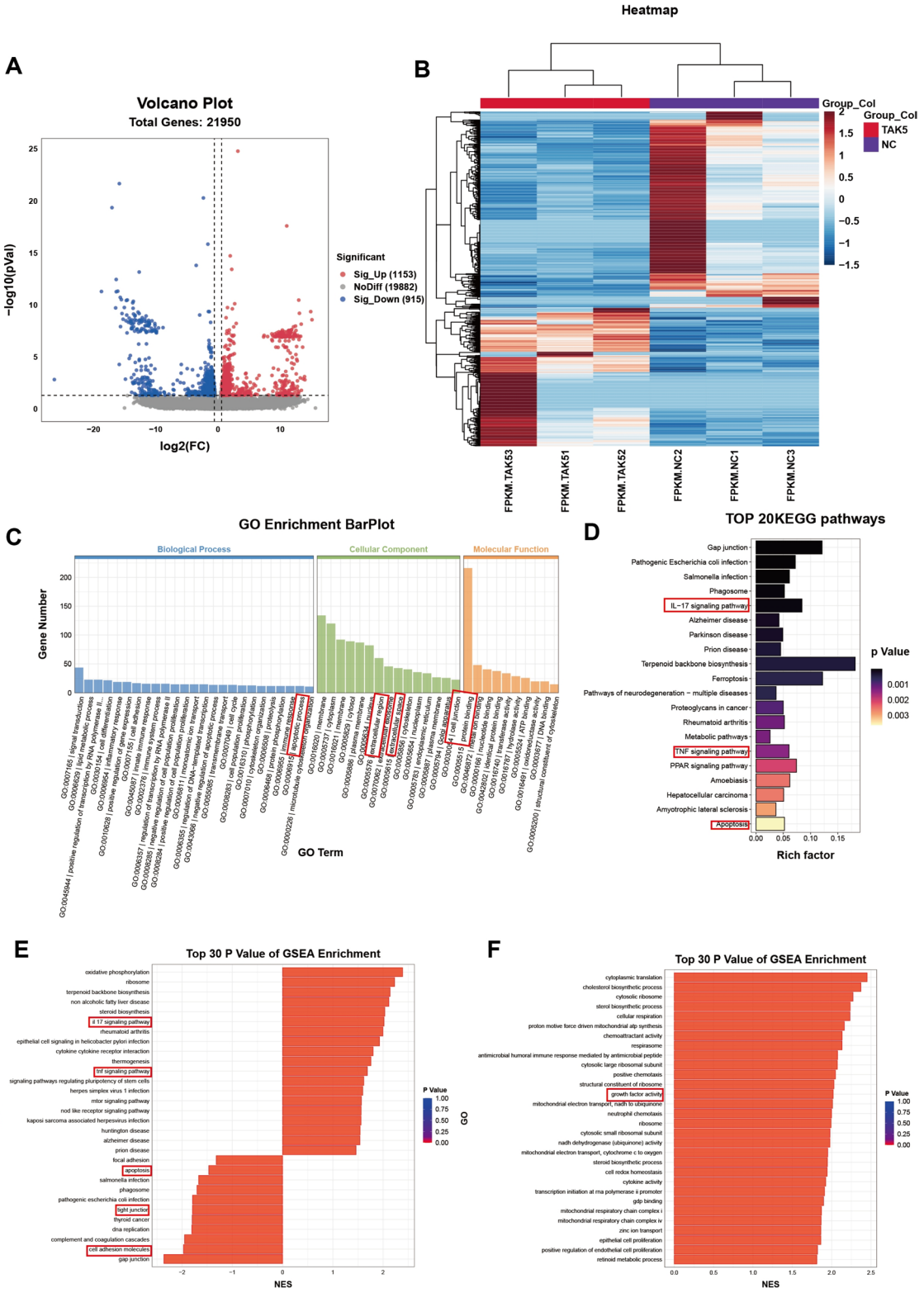

Fig. 5 (See legend on previous page.)

Finally, considering the macrophage infiltration in FS tissue, we used CIBRTSORT algorithm to conduct immune infiltration analysis after the TAK715 intervention. We found M1 macrophage distributed less in TAK715 intervention compared with FS group.

Overall, our bioinformatic results of TAK715 intervention vs FS are corresponding with previous part. The anti-fibrosis, anti-inflammation and modulating polarization effects of TAK715 were verified at bioinformatic level.

Effects of TAK715 on Glenohumeral ROM and histological appearance

At first, the micro-CT scans of the OVX and CON group femurs were performed and the results confirmed that the osteoporosis rats were successfully constructed (Supplementary Fig. 2, A-C). Then none of the SD rats exhibited glenohumeral joint dislocations or fractures at the examination point. The shoulder X-rays and ROM measurements showed that the angles between the lateral border of scapula and medial border of humerus were significantly lower in the frozen shoulder model side (left shoulder) than the control side (right shoulder) both at neutral and abduction position in the FSCON and FSOVX groups (Fig. 7A-D). The FSOVX group exhibited significantly lower angles in the FS side, confirming that the frozen shoulder models were successfully established and the FSOVX group was more serious in the limitation of glenohumeral joint.

The study examined the effects of TAK715 on the limitation of glenohumeral joint in different groups. In the T-FSCON group, there were no significant differences in angles between the FS side and control side in abduction position, but in neutral position, the angles in the FS side were still significantly lower than the control side. Additionally, the mean difference between FS and control side in neutral position was lower in the T-FSCON group than in the FSCON group. In the T-FSOVX group, there were still significant differences between FS and control side both at neutral and abduction position. Compared with the FSOVX group, the mean difference between FS and control side was not significantly different at neutral position, but at abduction position, the mean difference was significantly lower. The results showed that in the NOVX group, TAK715 had a significant treatment effect in almost completely correcting the limitation of glenohumeral joint at abduction position. However, in the OVX group, TAK715 could not completely correct the limitation of glenohumeral joint but also exhibited a treatment effect to some extent (Fig. 7A-D).

After the SD rats were sacrificed, the shoulder joints were separated, which is composed of the synovium and the fibrous layer. We found that TAK715 had a significant treatment effect in reversing fibrosis and reducing inflammation in both T-FSCON and T-FSOVX groups. H&E-stained and IHC images showed a significant decrease in inflammation cells that infiltrated the capsular and a thinner fibrous layer after TAK715 treatment. Moreover, we found that the inflammation cells were more infiltrated in FSOVX group (Fig. 7E-G; Supplementary Fig. 4.A, B). Additionally, the pro-inflammation cytokines (IL-1β, IL-6 and TNF-α) were also more secreted in OVX-FS capsule than in NOVX-FS capsule by ELISA (Supplementary Fig. 4.C). Masson-stained images confirmed that collagen was less dense (Fig. 7F).

Above all, these results confirmed that TAK715 was effective in reversing FS fibrosis and resisting inflammation infiltration, which was consistent with in vivo experiments. Additionally, the FSOVX group exhibited more severe symptoms in limitation of ROM and histology compared to the FSCON group, and the FSOVS group was more difficult to correct.

TAK715 could protect the shoulder osteoporosis to some extent

The study aimed to investigate the anti-osteoporosis effect of TAK715 in vitro and vivo. First, BMDMs were harvested and analyzed using flow cytometry, which were both F4/80 and CD11b positive, confirming successful macrophage induction (Fig. 8A). The TRAP-stained

(See figure on next page.)

Fig. 6 GSEA and immune infiltration analysis after TAK715 treatment. **A** The selected KEGG GSEA analysis ES diagram: apoptosis (pathway ID: hsa04210), TNF (pathway ID: hsa04668), IL-17 (pathway ID: hsa04657), MAPK signaling pathway (pathway ID: hsa04010) and TGF-beta signaling pathway (pathway ID: hsa04010). The combined ES diagram was at last. **B** The combined heatmap of selected pathways in KEGG GSEA analysis. **C** The selected GO GSEA analysis ES diagram: The collagen binding (GO:0005518), collagen-containing extracellular matrix (GO:0062023), collagen fiber organization (GO:0030199), growth factor activity (GO:0008083) and collagen trimer (GO:0005581). The combined ES diagram was at last. **D** The combined heatmap of selected pathways in KEGG GO analysis. **E** The inflammation-collagen interaction chord gram showed that the collagen terms and inflammation pathways are tightly linked. The value between term and pathway was calculated according to the $\log_2$ fold change of common genes. **F** The heatmap of different immune-cell gene expression in this gene set. The M1 macrophage related genes were more expressed in untreated FS synovial fibroblasts (NC group) compared with TAK715 treated (TAK5 group). **G** The correlation and *p* value of immune infiltration result. The M1 macrophage cluster exhibited the correlation of 0.18 and *p* value of 0.32, which indicated that the M1 macrophage infiltration was positive linked with the FS synovial fibroblasts

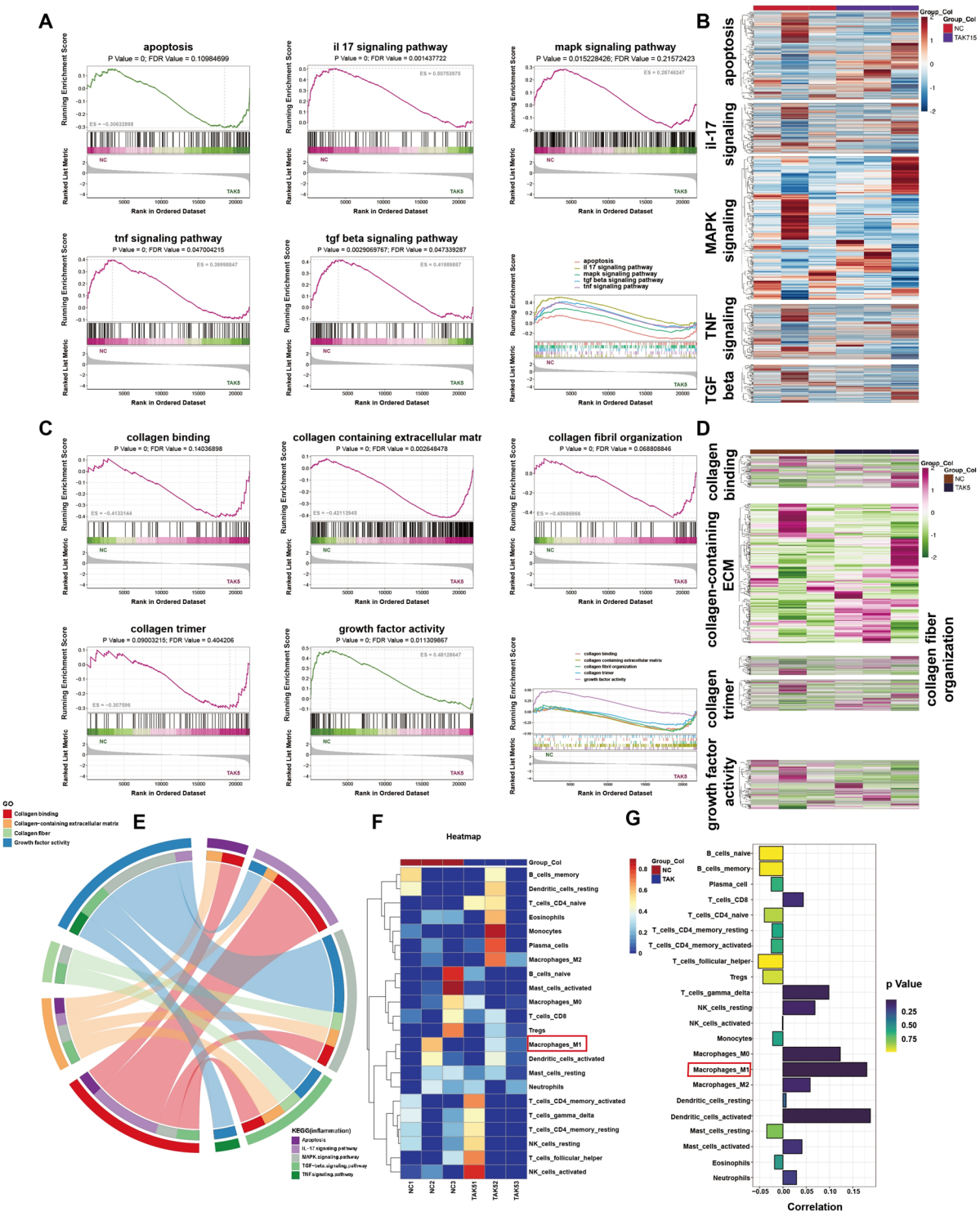

Fig. 6 (See legend on previous page.)

results showed that TAK715 (5 μM) could inhibit osteoclast activation after 5 days of RANKL induction at 30 ng/ml (Fig. 8B, C). Simultaneously, the TAK715 effect on osteoblast function was also tested by Alizarin red S(ARS) staining. The TAK715 at 5 μM didn't influence the osteoblast function (Fig. 8B, C).

In micro-CT examination, both the FSOVX and FSCON groups showed lower BMD on the FS side

compared to the control side, indicating local osteoporosis in FS patients. Furthermore, the study found that TAK715 could partially correct the local osteoporosis in both CON and OVX group (Fig. 8D-G). In the TRAP (tartrate-resistant acid phosphatase) staining, the more osteoclasts were accumulated in the epiphysis of FS side. Compared with the NOVX group, the OVX group also showed more accumulated osteoclasts. TAK715 could inhibit the osteoclast activation in vivo (Fig. 8D-G).

Discussion

The susceptibility to frozen shoulder aligns with that of osteoporosis, particularly affecting post-menopausal women. However, current research tends to view frozen shoulder (FS) and osteoporosis (OP) as distinct conditions due to insufficient evidence to suggest otherwise. Despite this, FS patients are at risk of developing local osteoporosis, as confirmed by previous studies [13, 14]. In our clinical observations, post-menopausal women constitute the majority of FS patients and often present with more severe symptoms. Additionally, during arthroscopic surgery, we noted that rotator cuff tears in FS patients were more amenable to anchoring, a finding consistent with existing literature.

Based on these clinical phenomena, this study sought to explore the nexus between FS and OP. By analyzing datasets from the Gene Expression Omnibus (GEO) database, we identified significant enrichment of the MAPK signaling pathway in both conditions. Our findings indicated heightened activity of the p38 MAPK pathway in FS at both tissue and cellular levels. Treatment with TAK715, a p38 inhibitor, mitigated fibrosis in FS synovial fibroblasts and hindered osteoclast activation. FS tissues showed increased rates of cellular apoptosis, with the presence of M1 macrophages and pro-inflammatory cytokines. TAK715 also modulated macrophage polarization. Animal studies confirmed the presence of local osteoporosis in FS and demonstrated TAK715's efficacy in alleviating shoulder osteoporosis. Collectively, the study underscores the significance of the p38 MAPK pathway and the therapeutic potential of TAK715 in FS. Notably, this is the first study to emphasize the connection between OP and FS.

Frozen shoulder (FS) can be categorized as primary or secondary, with primary FS occurring spontaneously without a clear cause and secondary FS linked to surgery or trauma [4, 8]. Various mechanisms of secondary FS pathogenesis have been proposed, including trauma, inflammation, and homeostatic imbalance [4, 52]. Primary FS lacks a specific etiology, with its initial phase associated with risk factors common to secondary FS. Although the pathogenesis of primary and secondary FS differs slightly, their clinical manifestations are largely indistinguishable [4]. The condition typically evolves through three overlapping phases: inflammation, stiffness, and resolution. Inflammation and fibrosis are central to FS pathogenesis. Our previous work confirmed that IL-6 promotes FS fibrosis via the PI3K-Akt signaling pathway [12], and Salvianolic acid B mitigates inflammation and pathological fibrosis by inhibiting CD36-mediated activation of the PI3K-Akt pathway in FS. The MAPK signaling pathway, crucial in cellular adhesion and inflammation response, was significantly enriched in previous studies [53], and our bioinformatic analysis corroborated these findings. Regarding osteoporosis, it is a systemic skeletal disease characterized by compromised bone microarchitecture and increased fragility. Despite identifying several risk factors (such as estrogen deficiency or aging), osteoporosis remains prevalent.

In this study, we concentrated on the p38 MAPK signaling pathway's role in FS pathogenesis. Given p38 MAPK's link to cellular apoptosis, we investigated its role in FS pathogenesis. The apoptosis process was similarly active as observed in liver fibrosis [54, 55]. We also collected glenohumeral joint fluid from FS and control patients to measure pro-inflammatory cytokines. Since TNF-α showed the most significant difference, its role as a fibrogenic stimulus was confirmed. Under TNF-α stimulation, apoptosis indices increased, indicating that pro-inflammatory cytokine stimulation could trigger apoptosis and fibrosis in synovial fibroblasts via the p38 MAPK pathway.

TAK715, an oral and specific p38 MAPK inhibitor with an IC50 of 7.1 nM for p38α, has been shown to ameliorate rat arthritis in vivo [39]. Moreover, TAK715 reduced intervertebral disc degeneration in vitro and in vivo

(See figure on next page.)

Fig. 7 the X-ray images (**A**, **B**), ROM measurement (**C**, **D**) and histology analysis of FS rat models. **A**, **B** The X-rays of FS rats in neutral and abduction position and the statistics analysis of angle measurement in (**A**). ($n=6$) *$P<0.05$; **$P<0.01$; *** $P<0.001$; **** $P<0.0001$. **C**, **D** The ROM measurement of FS rats in neutral and abduction position and the statistics analysis of ROM measurement in (**A**). ($n=6$) *$P<0.05$; **$P<0.01$; *** $P<0.001$; **** $P<0.0001$. **E** Representative hematoxylin and eosin-stained (H&E) tissue sections of the shoulder joint. The capsule regions were encircled in dotted rectangle. Scale Bar: 100 μM. **F** Representative masson-stained tissue sections of the shoulder joint. The capsule regions were encircled in dotted rectangle. Scale Bar: 100 μM. **G** The statistics analysis of capsular thickness(mm) and macrophage relative counts in (**E**). ($n=3$) *$P<0.05$; **$P<0.01$; *** $P<0.001$; **** $P<0.0001$

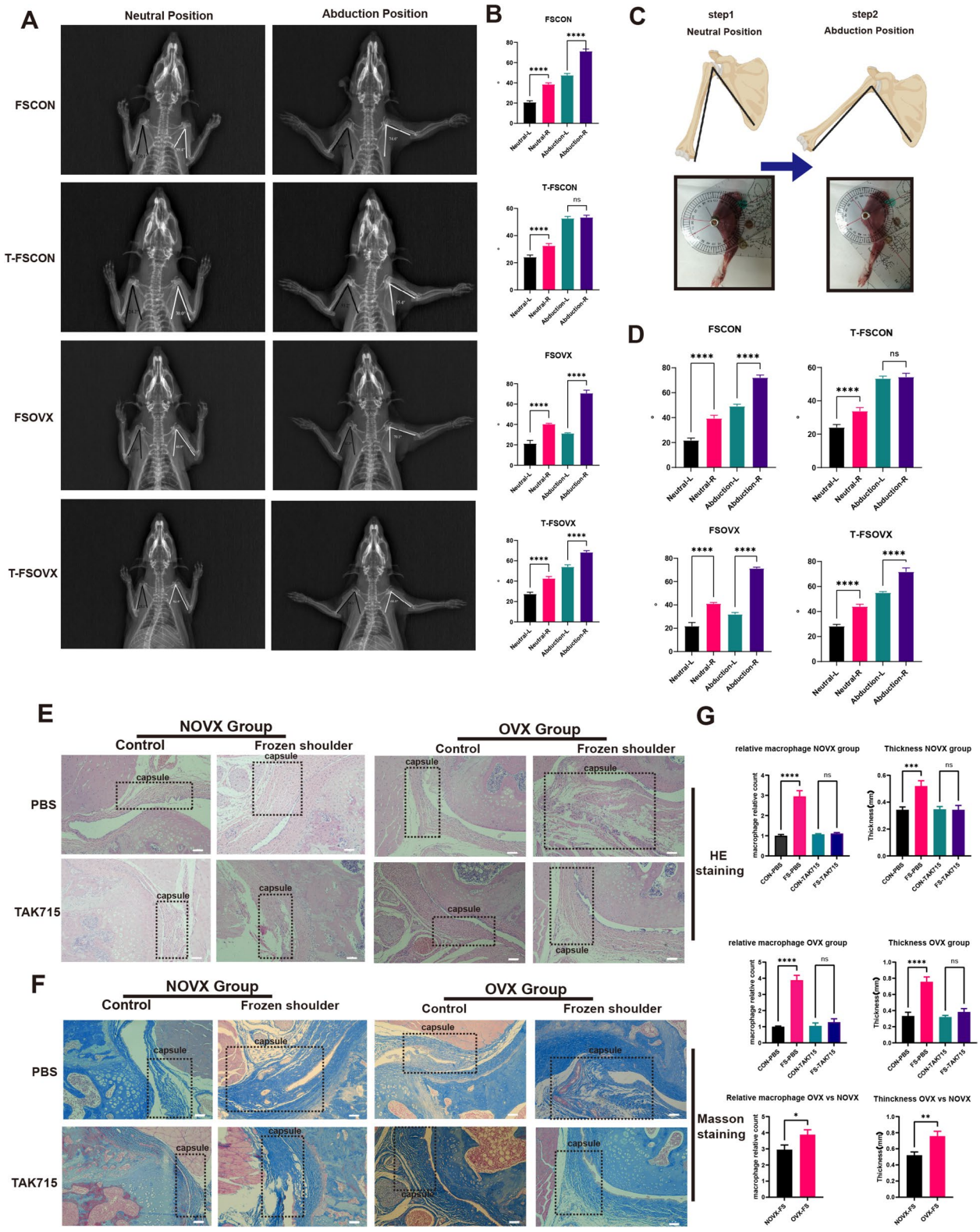

Fig. 7 (See legend on previous page.)

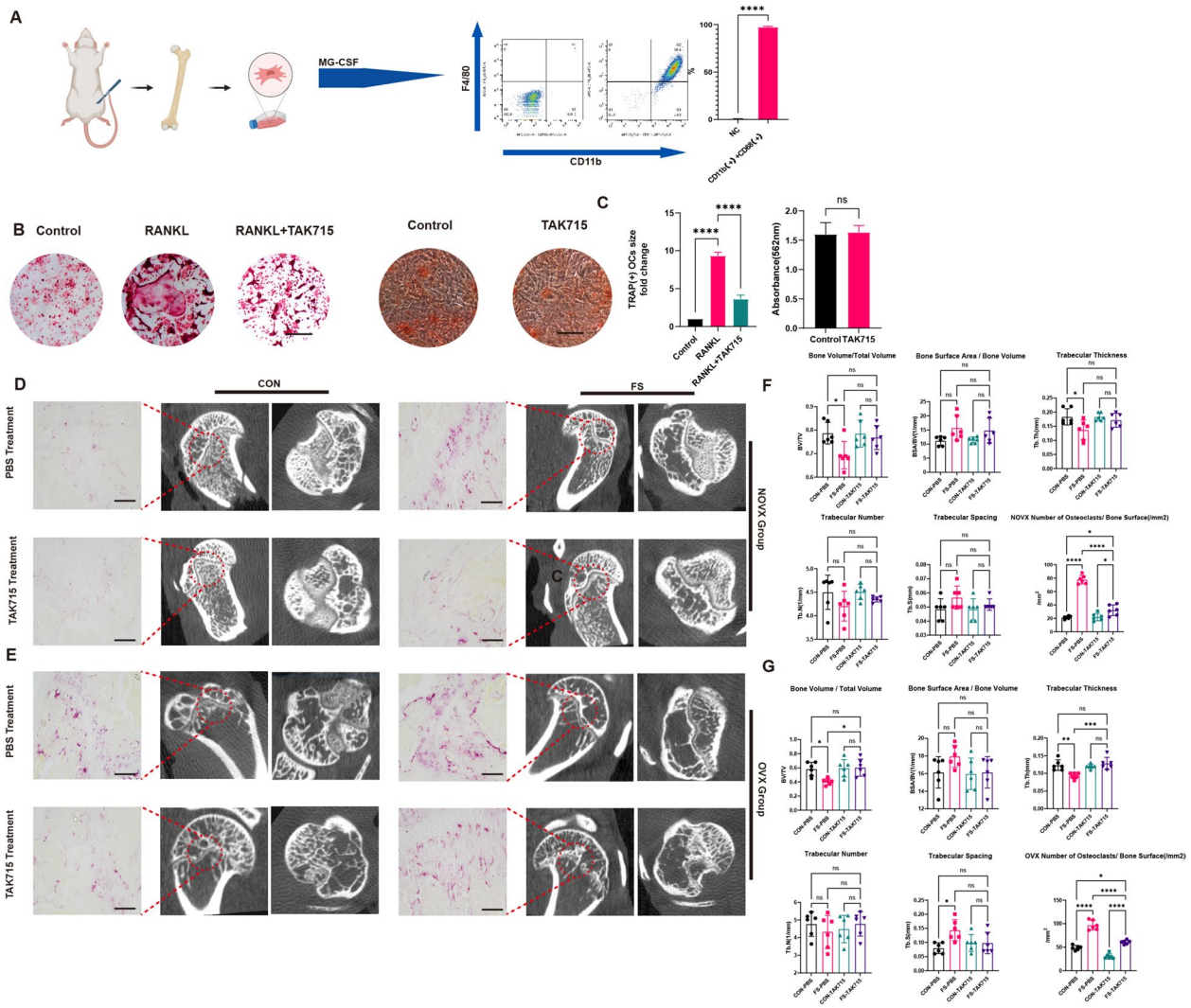

Fig. 8 the TAK715 could interpose the osteoclast activation and protect the osteoporosis. **A** The monocytes were successfully harvested from the rat bone marrow. **B**, **C** The osteoclasts were successfully induced by RANKL and the TAK715 could interpose the osteoclast activation at the concentration of 5 μM and the Alizarin red S(ARS) staining confirmed that TAK715 didn't influence the bone formation ability at 5 μM. Scale Bar: 50 μm. **D**, **E** The FS side exhibit a local osteoporosis and more active osteoclasts both in control and OVX group and with the treatment of TAK715 the local osteoporosis in FS side could be corrected. Scale Bar: 200 μm. **F**, **G** The statistic results ($n = 6$) of Bone Volume/Total Volume, Trabecular number, Trabecular spacing, Trabecular thickness, Bone surface area/ Bone Volume and Number of Osteoclasts/ Bone Surface(/mm2) in Fig. 8 (**D**, **E**)

through anti-inflammatory mechanisms. In this study, TAK715 demonstrated remarkable efficacy in correcting fibrosis and osteoporosis both in vitro and in vivo. Based on TAK715's treatment effects, we found that p38 MAPK activation was associated with fibrosis progression in synovial fibroblasts, independent of inflammation. Thus, we propose that FS fibrosis comprises two components: inflammation-induced fibrosis and intrinsic fibrosis not triggered by inflammation.

Frozen shoulder (FS) is characterized by reversible fibrosis, particularly during the resolution phase. FS fibrosis intensifies between the inflammation and stiffness phases. Interestingly, FS patients may experience spontaneous relief during the resolution phase, unlike other fibrotic diseases such as pulmonary, renal, and liver fibrosis. Based on our results, we hypothesize that fibrogenic stimuli, such as TNF-α, are released in the glenohumeral joint due to intrinsic or extrinsic factors like trauma, hormonal imbalance, or metabolic diseases. This triggers p38 MAPK, leading to imbalanced cellular apoptosis. Local cellular apoptosis or trauma attracts macrophages, prompting inflammation and fibrosis progression. The patient then enters the inflammatory phase. As fibrotic proteins accumulate, the stiffness phase

occurs. Ultimately, with the cessation of fibrogenic stimuli and consistent cellular apoptosis, synovial fibroblasts cease secretion, and fibrotic proteins are degraded by M1 macrophages [55, 56]. This could explain the resolution phase in FS patients.

Current research primarily focuses on this reversible fibrosis, but osteoporosis in FS is often overlooked. Previous studies have reported local osteoporosis in the humeral head of FS shoulders. We speculate that this osteoporosis results from partial immobilization of the glenohumeral joint and inflammation infiltration, leading to overactive osteoclasts and increased bone resorption. Shoulder osteoporosis raises the risk of pathological fractures, especially in postmenopausal women, who have a higher incidence of FS. Our results first confirmed that the FS side exhibited more osteoporosis than the control side, aligning with clinical findings. Moreover, ovariectomized (OVX) rats displayed more severe FS symptoms, suggesting that osteoporosis might be a risk factor for FS or exacerbate its symptoms. The p38 MAPK pathway is crucial for osteoclast maturation, and our results verified that TAK715 effectively inhibits osteoclast maturation in vitro. In animal experiments, rats treated with TAK715 showed less osteoporosis. We believe TAK715 is potent in protecting against osteoporosis by preventing osteoclast maturation (as shown in Fig. 9).

Overall, this study aimed to investigate the relationship between frozen shoulder and osteoporosis and to find a method to correct fibrosis and protect against osteoporosis simultaneously, marking a novel approach in FS research. We propose that the p38 MAPK signaling pathway may be the intersection between fibrosis and osteoporosis. The specific p38 inhibitor TAK715 was effective in correcting fibrosis and protecting against osteoporosis (as shown in Fig. 9).

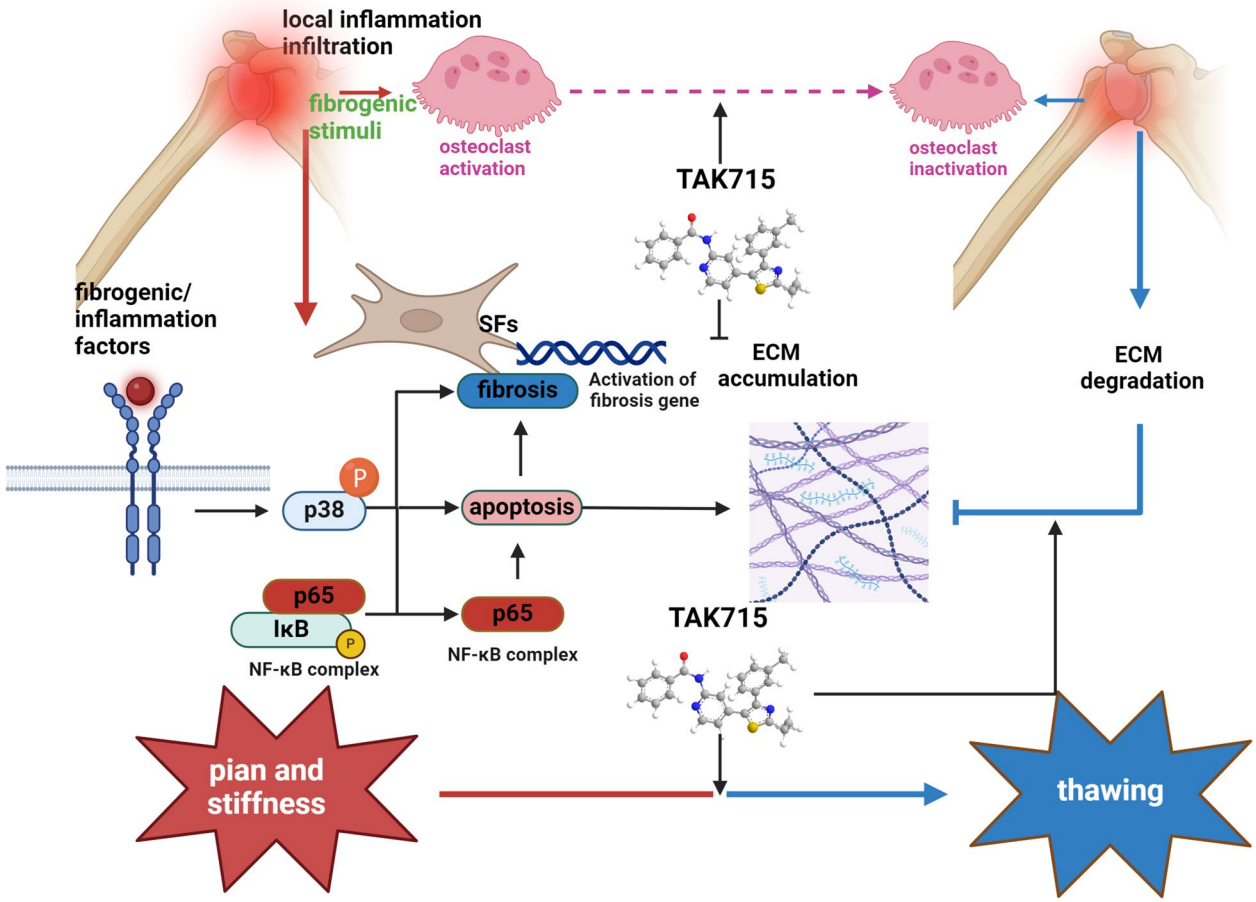

Fig. 9 The pathogenesis mechanism based on the activation of p38 MAPK signal pathway and the therapeutic effect of TAK715. Briefly, the extrinsic or intrinsic reasons produced fibrogenic stimuli and the stimuli triggered synovium fibroblast apoptosis and recruited macrophage infiltration. At the initial pathogenesis phase, the osteoclast was also activated. In this stage, the patients suffered from pain, stiffness and bone loss. Under the cessation of fibrogenic stimuli and consistent cell apoptosis, the ECM secreting is stopped and degraded. The FS comes into thawing phase. Holistically, the TAK715 could correct the fibrosis and local osteoporosis to accelerate the rehabilitation. (Created from https://www.biorender.com)

However, this study has limitations. First, although we confirmed the crosstalk genes and the role of the p38 MAPK signaling pathway linking FS and OP, the deeper correlation between them requires further investigation. Despite examining clinical phenomena and developing animal models, there are inherent differences between humans and rats. Additionally, while our hypothesis about FS pathogenesis during the resolution phase is theoretically sound, practical validation is needed. Due to the difficulty of obtaining tissue samples during the resolution phase, our results only partially confirm the hypothesis. Furthermore, whether bone mineral density changes after OVX significantly influence the FS process requires further research. The mechanism by which TAK715 protects against osteoporosis is unclear; it may primarily inhibit osteoclast activation directly or correct FS to indirectly affect osteoclasts. For future research, potential targets or functions associated with p38 MAPK should be explored, and the long-term therapeutic effects of TAK715 or other drugs targeting p38 MAPK in vitro or in vivo need clarification. Finally, conducting randomized clinical controlled trials or clinical translational research would be highly valuable.

Conclusion

Overall, this study explores the connection FS and OP and provides a new and available theory about the pathogenesis process of frozen shoulder based on the p38 MAPK signal pathway. The frozen shoulder with osteoporosis may exhibit more severe symptoms in animal experiments, and TAK715 is effective in protecting fibrosis and osteoporosis both in vitro and vivo.

Abbreviations

FS	Frozen Shoulder
OP	Osteoporosis
SF	Synovium fibroblast
qRT-PCR	Quantitative real time polymerase chain reaction
BMDMs	Bone Marrow Derived Macrophages
ROM	Range of motion
ECM	Extracellular matrix
BV/TV	The Bone Volume/Total Volume
BSA/BV	Bone Surface Area/Bone Volume
Tb.Th	Trabecular Thickness
Tb.N	Trabecular number
Tb.S	Trabecular

Supplementary Information

The online version contains supplementary material available at https://doi.org/10.1186/s12891-024-08068-8.

Supplementary Material 1.

Supplementary Material 2.

Supplementary Material 3.

Supplementary Material 4.

Acknowledgements

We gratefully acknowledge Weike Zeng and Huijun Hu from the Department of Radiology, the Sun Yat-sen Memorial Hospital of Sun Yat-sen University, Qingqiang Tu and Min Zhou from Sun Yat-sen University for providing guidance on X-ray and CT imaging.

Authors' contributions

Rui Yang, Ming Li and Xinhao Li made conception and design; Xinhao Li, Yan Yan, Zhuo Wang, Jingyi Hou, Yuhan Meng and Dedong Cui collected the data; Ming Li and Rui Yang provided technique support; Xinhao Li, Yan Yan and Yi Long analysis the data; Xinhao Li, Yan Yan and Zhuo Wang finished writing the manuscript. Yi Long and Ming Li review and corrected the manuscript.

Funding

This work was supported by the National Natural Science Foundation of China (NO.81972067) and the Fundamental Research Funds for the Central Universities, Sun Yat-sen University (NO.2020004).

Data availability

Data is provided within the manuscript or supplementary information files. The RNA-seq data was uploaed to GEO database (GSE265890). Additionaly, the data that support the findings of this study are available from the corresponding author upon reasonable request.

Declarations

Ethics approval and consent to participate

The studies involving human participants were reviewed and approved by Ethics Committee of the Sun Yat-sen Memorial Hospital of Sun Yat-sen University (SYSKY-2023–1110-01). The patients/participants provided their written informed consent to participate in this study. All animal care and experimental procedures were performed following the guidelines of the care and use of laboratory animals approved by the Sun Yat-sen Memorial Hospital of Sun Yat-sen University Institutional Animal Care and Use Committee and ARRIVE guidelines. The approval number is SYSU-IACUC-2021–000931.

Consent for publication

Not applicable.

Competing interests

The authors declare no competing interests.

Author details

[1]Department of Orthopedics and Department of Sports Medicine, Sun Yat-Sen Memorial Hospital, Sun Yat-Sen University, 107# Yanjiang West Road, Guangzhou, Guangdong Province 510120, China. [2]Division of Life Sciences and Medicine, The First Affiliated Hospital of USTC, University of Science and Technology of China, #17 Lujiang Road, Hefei, Anhui Province, China.

Received: 9 April 2024 Accepted: 13 November 2024
Published online: 21 November 2024

References

1. Riley D, Lang AE, Blair RD, Birnbaum A, Reid B. Frozen shoulder and other shoulder disturbances in Parkinson's disease. J Neurol Neurosurg Psychiatry. 1989;52(1):63–6.
2. Koorevaar RCT, Van't Riet E, Ipskamp M, Bulstra SK. Incidence and prognostic factors for postoperative frozen shoulder after shoulder surgery: a prospective cohort study. Arch Orthop Trauma Surg. 2017;137(3):293–301.
3. Cho CH, Lee KL, Cho J, Kim D. The incidence and risk factors of frozen shoulder in patients with breast cancer surgery. Breast J. 2020;26(4):825–8.
4. Millar NL, Meakins A, Struyf F, Willmore E, Campbell AL, Kirwan PD, Akbar M, Moore L, Ronquillo JC, Murrell GAC, et al. Frozen shoulder. Nat Rev Dis Primers. 2022;8(1):59.

5. Cho CH, Lee YH, Kim DH, Lim YJ, Baek CS, Kim DH. Definition, Diagnosis, Treatment, and Prognosis of Frozen Shoulder: A Consensus Survey of Shoulder Specialists. Clin Orthop Surg. 2020;12(1):60–7.
6. Brun SP. Idiopathic frozen shoulder. Aust J Gen Pract. 2019;48(11):757–61.
7. Karbowiak M, Holme T, Mirza M, Siddiqui N. Frozen shoulder. Bmj. 2022;377: e068547.
8. Dias R, Cutts S, Massoud S. Frozen shoulder. BMJ. 2005;331(7530):1453–6.
9. Ramirez J. Adhesive Capsulitis: Diagnosis and Management. Am Fam Physician. 2019;99(5):297–300.
10. Akbar M, McLean M, Garcia-Melchor E, Crowe LA, McMillan P, Fazzi UG, Martin D, Arthur A, Reilly JH, McInnes IB, et al. Fibroblast activation and inflammation in frozen shoulder. PLoS ONE. 2019;14(4): e0215301.
11. Cho CH, Song KS, Kim BS, Kim DH, Lho YM. Biological Aspect of Pathophysiology for Frozen Shoulder. Biomed Res Int. 2018;2018:7274517.
12. Yang R, Tang Y, Hou J, Yu M, Long Y, Yamuhanmode A, Li Q, Li F, Zhang Y, Warsame M, et al. Fibrosis in frozen shoulder: Activation of IL-6 through PI3K-Akt signaling pathway in synovial fibroblast. Mol Immunol. 2022;150:29–38.
13. Okamura K, Ozaki J. Bone mineral density of the shoulder joint in frozen shoulder. Arch Orthop Trauma Surg. 1999;119(7–8):363–7.
14. Leppälä J, Kannus P, Sievänen H, Järvinen M, Vuori I. Adhesive capsulitis of the shoulder (frozen shoulder) produces bone loss in the affected humerus, but long-term bony recovery is good. Bone. 1998;22(6):691–4.
15. Poston L, Caleyachetty R, Cnattingius S, Corvalán C, Uauy R, Herring S, Gillman MW. Preconceptional and maternal obesity: epidemiology and health consequences. Lancet Diabetes Endocrinol. 2016;4(12):1025–36.
16. Xiao PL, Cui AY, Hsu CJ, Peng R, Jiang N, Xu XH, Ma YG, Liu D, Lu HD. Global, regional prevalence, and risk factors of osteoporosis according to the World Health Organization diagnostic criteria: a systematic review and meta-analysis. Osteoporos Int. 2022;33(10):2137–53.
17. Struyf F, Mertens MG, Navarro-Ledesma S: Causes of Shoulder Dysfunction in Diabetic Patients: A Review of Literature. *Int J Environ Res Public Health* 2022, 19(10).
18. Gundtoft PH, Attrup ML, Kristensen AK, Vobbe JW, Sørensen L, Hölmich P: Diabetes mellitus affects the prognosis of frozen shoulder. *Dan Med J* 2020, 67(10).
19. Wang JP, Huang TF, Hung SC, Ma HL, Wu JG, Chen TH. Comparison of idiopathic, post-trauma and post-surgery frozen shoulder after manipulation under anesthesia. Int Orthop. 2007;31(3):333–7.
20. Itoi E, Arce G, Bain GI, Diercks RL, Guttmann D, Imhoff AB, Mazzocca AD, Sugaya H, Yoo YS. Shoulder Stiffness: Current Concepts and Concerns. Arthroscopy. 2016;32(7):1402–14.
21. Safran O, El-Haj M, Leibowitz G, Beyth S, Furman Z, Milgrom C, Kandel L. Should Patients With Frozen Shoulder Be Screened for Diabetes Mellitus? Orthop J Sports Med. 2017;5(7):2325967117716450.
22. Dyer BP, Rathod-Mistry T, Burton C, van der Windt D, Bucknall M. Diabetes as a risk factor for the onset of frozen shoulder: a systematic review and meta-analysis. BMJ Open. 2023;13(1): e062377.
23. Rodeo SA, Hannafin JA, Tom J, Warren RF, Wickiewicz TL. Immunolocalization of cytokines and their receptors in adhesive capsulitis of the shoulder. J Orthop Res. 1997;15(3):427–36.
24. Millar NL, Silbernagel KG, Thorborg K, Kirwan PD, Galatz LM, Abrams GD, Murrell GAC, McInnes IB, Rodeo SA. Tendinopathy. Nat Rev Dis Primers. 2021;7(1):1.
25. Sun Y, Lin J, Luo Z, Zhang Y, Chen J. The Serum from Patients with Secondary Frozen Shoulder Following Rotator Cuff Repair Induces Shoulder Capsule Fibrosis and Promotes Macrophage Polarization and Fibroblast Activation. J Inflamm Res. 2021;14:1055–68.
26. Akbar M, Crowe LAN, McLean M, Garcia-Melchor E, MacDonald L, Carter K, Fazzi UG, Martin D, Arthur A, Reilly JH *et al*: Translational targeting of inflammation and fibrosis in frozen shoulder: Molecular dissection of the T cell/IL-17A axis. *Proc Natl Acad Sci U S A* 2021, 118(39).
27. Yu B, Wang CY: Osteoporosis and periodontal diseases - An update on their association and mechanistic links. *Periodontol 2000* 2022, 89(1):99–113.
28. Wu D, Cline-Smith A, Shashkova E, Perla A, Katyal A, Aurora R. T-Cell Mediated Inflammation in Postmenopausal Osteoporosis. Front Immunol. 2021;12: 687551.
29. Tao H, Li W, Zhang W, Yang C, Zhang C, Liang X, Yin J, Bai J, Ge G, Zhang H, et al. Urolithin A suppresses RANKL-induced osteoclastogenesis and postmenopausal osteoporosis by, suppresses inflammation and downstream NF-κB activated pyroptosis pathways. Pharmacol Res. 2021;174: 105967.
30. Wagner EF, Nebreda AR. Signal integration by JNK and p38 MAPK pathways in cancer development. Nat Rev Cancer. 2009;9(8):537–49.
31. Cuadrado A, Nebreda AR. Mechanisms and functions of p38 MAPK signalling. Biochem J. 2010;429(3):403–17.
32. Yong HY, Koh MS, Moon A. The p38 MAPK inhibitors for the treatment of inflammatory diseases and cancer. Expert Opin Investig Drugs. 2009;18(12):1893–905.
33. Coulthard LR, White DE, Jones DL, McDermott MF, Burchill SA. p38(MAPK): stress responses from molecular mechanisms to therapeutics. Trends Mol Med. 2009;15(8):369–79.
34. Yue J, López JM: Understanding MAPK Signaling Pathways in Apoptosis. In: *International Journal of Molecular Sciences.* vol. 21; 2020.
35. Rodríguez-Carballo E, Gámez B, Ventura F. p38 MAPK Signaling in Osteoblast Differentiation. Front Cell Dev Biol. 2016;4:40.
36. Koga Y, Tsurumaki H, Aoki-Saito H, Sato M, Yatomi M, Takehara K, Hisada T: Roles of Cyclic AMP Response Element Binding Activation in the ERK1/2 and p38 MAPK Signalling Pathway in Central Nervous System, Cardiovascular System, Osteoclast Differentiation and Mucin and Cytokine Production. *Int J Mol Sci* 2019, 20(6).
37. Falck D, Kool J, Honing M, Niessen WM. Tandem mass spectrometry study of p38α kinase inhibitors and related substances. J Mass Spectrom. 2013;48(6):718–31.
38. Falck D, de Vlieger JS, Niessen WM, Kool J, Honing M, Giera M, Irth H. Development of an online p38α mitogen-activated protein kinase binding assay and integration of LC-HR-MS. Anal Bioanal Chem. 2010;398(4):1771–80.
39. Miwatashi S, Arikawa Y, Kotani E, Miyamoto M, Naruo K, Kimura H, Tanaka T, Asahi S, Ohkawa S. Novel inhibitor of p38 MAP kinase as an anti-TNF-alpha drug: discovery of N-[4-[2-ethyl-4-(3-methylphenyl)-1,3-thiazol-5-yl]-2-pyridyl]benzamide (TAK-715) as a potent and orally active anti-rheumatoid arthritis agent. J Med Chem. 2005;48(19):5966–79.
40. Yan Y, Zhou M, Meng K, Zhou C, Jia X, Li X, Cui D, Yu M, Tang Y, Li M, et al. Salvianolic acid B attenuates inflammation and prevent pathologic fibrosis by inhibiting CD36-mediated activation of the PI3K-Akt signaling pathway in frozen shoulder. Front Pharmacol. 2023;14:1230174.
41. Deng YX, He WG, Cai HJ, Jiang JH, Yang YY, Dan YR, Luo HH, Du Y, Chen L, He BC. Analysis and Validation of Hub Genes in Blood Monocytes of Postmenopausal Osteoporosis Patients. Front Endocrinol (Lausanne). 2021;12: 815245.
42. Hu Y, Han J, Ding S, Liu S, Wang H. Identification of ferroptosis-associated biomarkers for the potential diagnosis and treatment of postmenopausal osteoporosis. Front Endocrinol (Lausanne). 2022;13: 986384.
43. Yang C, Ren J, Li B, Jin C, Ma C, Cheng C, Sun Y, Shi X. Identification of gene biomarkers in patients with postmenopausal osteoporosis. Mol Med Rep. 2019;19(2):1065–73.
44. Percie du Sert N, Ahluwalia A, Alam S, Avey MT, Baker M, Browne WJ, Clark A, Cuthill IC, Dirnagl U, Emerson M *et al*: Reporting animal research: Explanation and elaboration for the ARRIVE guidelines 2.0. *PLoS Biol* 2020, 18(7):e3000411.
45. Zhao H, Kong L, Shen J, Ma Y, Wu Z, Li H, He Y. Tetrandrine inhibits the occurrence and development of frozen shoulder by inhibiting inflammation, angiogenesis, and fibrosis. Biomed Pharmacother. 2021;140: 111700.
46. Jang HY, Kim GB, Kim JM, Kang SY, Youn HJ, Park J, Ro SY, Chung EY, Park KH, Kim JS: Fisetin Inhibits UVA-Induced Expression of MMP-1 and MMP-3 through the NOX/ROS/MAPK Pathway in Human Dermal Fibroblasts and Human Epidermal Keratinocytes. *Int J Mol Sci* 2023, 24(24).
47. Wang Y, Wang B, Cao W, Xu X. PTX3 activates POSTN and promotes the progression of glioblastoma via the MAPK/ERK signalling axis. Biochem Biophys Res Commun. 2024;703: 149665.
48. Li F, Tang Y, Song B, Yu M, Li Q, Zhang C, Hou J, Yang R. Nomenclature clarification: synovial fibroblasts and synovial mesenchymal stem cells. Stem Cell Res Ther. 2019;10(1):260.
49. Herrmann FE, Hesslinger C, Wollin L, Nickolaus P. BI 1015550 is a PDE4B Inhibitor and a Clinical Drug Candidate for the Oral Treatment of Idiopathic Pulmonary Fibrosis. Front Pharmacol. 2022;13: 838449.
50. Jing F, Chen X, Xue J, Huang K, Xing F, Hu X, Peng Y, Liu C. An Herbal Product Alleviates Bleomycin-Induced Pulmonary Fibrosis in Mice via

Regulating NF-κB/TNF-α Signaling in Macrophages. Front Pharmacol. 2022;13: 805432.
51. Wen Y, Rudemiller NP, Zhang J, Robinette T, Lu X, Ren J, Privratsky JR, Nedospasov SA, Crowley SD. TNF-α in T lymphocytes attenuates renal injury and fibrosis during nephrotoxic nephritis. Am J Physiol Renal Physiol. 2020;318(1):F107-f116.
52. Ryan V, Brown H, Minns Lowe CJ, Lewis JS. The pathophysiology associated with primary (idiopathic) frozen shoulder: A systematic review. BMC Musculoskelet Disord. 2016;17(1):340.
53. Kamal N, McGee SL, Eng K, Brown G, Beattie S, Collier F, Gill S, Page RS. Transcriptomic analysis of adhesive capsulitis of the shoulder. J Orthop Res. 2020;38(10):2280–9.
54. Weiskirchen R, Weiskirchen S, Tacke F. Organ and tissue fibrosis: Molecular signals, cellular mechanisms and translational implications. Mol Aspects Med. 2019;65:2–15.
55. Kisseleva T, Brenner D. Molecular and cellular mechanisms of liver fibrosis and its regression. Nat Rev Gastroenterol Hepatol. 2021;18(3):151–66.
56. Wolf MT, Dearth CL, Ranallo CA, LoPresti ST, Carey LE, Daly KA, Brown BN, Badylak SF. Macrophage polarization in response to ECM coated polypropylene mesh. Biomaterials. 2014;35(25):6838–49.

Publisher's Note